

# Measurements of seismic wave attenuation using multiple ScS waves

Honor's thesis

Joshua C. Miller

*Department of Earth and Environmental Sciences  
University of Michigan*

## Summary

The seismic quality factor  $Q$  is a measure of seismic wave attenuation due to the earth's anelasticity. In most global models,  $Q$  has a value of about 300-500 in the lower mantle. Recently, *Kanamori and Rivera* (2015) estimated a remarkably high value of  $Q$  of 1400 beneath global seismic network station AFI on Samoa using ratios of peak-to-peak amplitudes of multiple ScS phases generated by earthquakes in Tonga. This indicates that shear-wave attenuation throughout the mantle in the region is very low. We follow up on this study by analyzing waveforms from stations AFI and EUAT of the March 9, 1994 Tonga earthquake with a different analytical approach: (1) we measure amplitude ratios from waveform cross correlation coefficients, (2) we include surface reflections sScS and its multiples, (3) we estimate  $Q$  in the upper and lower mantle separately. We confirm *Kanamori and Rivera's* (2015) estimate of a high  $Q$  value at AFI and estimate that  $Q = 2000$  for both the upper and lower mantle. For station EUAT with sampling of the Lau Basin, we find that  $Q$  may be lower in the upper mantle, but a complete follow-up analysis must confirm the resolution of upper mantle attenuation using ScS phases.

## 1. Introduction

The amplitude is a fundamental attribute of a (seismic) wave. Earthquake seismologists determine the magnitude (or seismic moment) of earthquakes from the amplitudes of seismic waves. Wave amplitudes have also been widely used in seismic studies of Earth structure. Classic studies of so-called shadow zones, with reduced wave amplitudes, and triplications, where wave amplitudes spike, have led to the discoveries of Earth's outer core and inner core, the crust-mantle interface, and phase transitions in Earth's mantle (see *Lay and Wallace, 1995*).

Amplitudes also provide constraints on scattering by small-scale compositional heterogeneity (i.e., *extrinsic* attenuation) and on the absorption of wave energy by grain-boundary friction and fluid movement (i.e., *intrinsic* attenuation) (*Knopoff, 1964*). Combined, scattering and absorption diminish seismic waves faster than geometric spreading alone. The reduction of the amplitude during wave propagation is often expressed by the seismic quality factor  $Q$  which quantifies the fractional energy lost per wave cycle.

$$Q^{-1} = \Delta E / (2\pi E_{max}), \quad (1)$$

where  $\Delta E$  is the elastic energy lost per wave cycle and  $E_{max}$  is the maximum elastic energy contained in a cycle.  $Q$  is the inverse of anelastic attenuation. When  $Q$  is high, damping is low, and, vice versa, when  $Q$  is low, damping is high. With this definition of  $Q$ , the reduction of the wave amplitude  $A$  due to attenuation is proportional to

$$A \sim e^{-\omega x / 2cQ}, \quad (2)$$

where  $\omega$  is angular frequency,  $x$  is the distance of wave propagation, and  $c$  is wave velocity, akin to the attenuation factor of a damped harmonic oscillator.

Figure 1 shows several estimates of the depth profile of  $Q_{\mu}$  for shear wave propagation (from hereon denoted simply as  $Q$ ) in the mantle. The profiles indicate a variation that broadly reflects the physical layering of the mantle.  $Q$  is highest in the lithosphere, the mechanically strong, thermal boundary layer, and lowest in the asthenosphere, the region of the mantle closest to the melting temperature. More localised studies of  $Q$  (e.g. *Shito and Shibutan, 2003*) as well as laboratory studies of rock deformation (e.g., *Faul and Jackson, 2005*), indicate that melt and water content and grain size are also important factors.

Studies of  $Q$  have intensified since the 1970s with the advent of well-calibrated, digital seismic instrumentation that accurately record wave amplitude over a wide frequency range. The most

recent global-scale maps of  $Q$  (e.g., *Dalton et al.*, 2007) illuminate active tectonic regions as low- $Q$  regions and stable continental interior as high- $Q$  regions. On regional scales,  $Q$  in the upper mantle has been found to vary laterally by an order of magnitude or more. For example, using a spectral decay method *Benz et al* (1997) reported that  $Q$  in the upper mantle varies from 187 below Southern California to 1291 below the central United States. Similar variations of  $Q$  have been inferred for South America: low  $Q$  values (250-450) are resolved along the western margin and high  $Q$  values ( $> 700$ ) are present in the interior of the continent (*DeSouza and Mitchell*, 1998). The same pattern holds for other continents (*Mitchell et al.*, 2007; *Mitchell et al.*, 1998; *Xie and Mitchell*, 1990), suggesting that  $Q$  varies as a function of tectonic age, with low  $Q$  values in terranes recently or concurrently undergoing tectonism, and high  $Q$  values in stable regions.

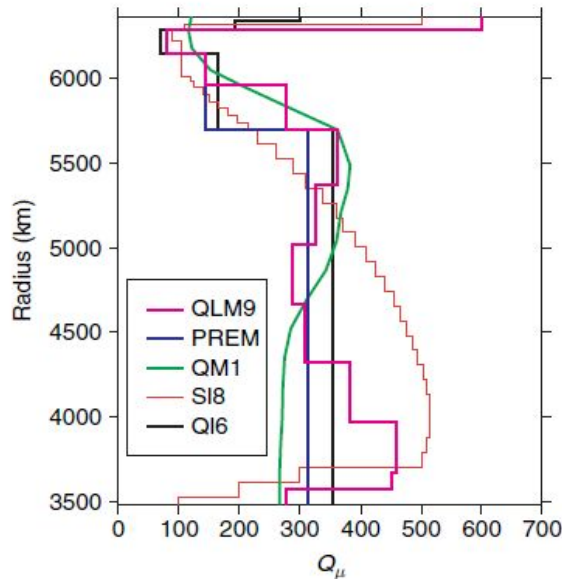


*Figure 1.* Profiles of  $Q_\mu$  (i.e.  $Q$  for S waves) as a function of radius (bottom is the core-mantle boundary; top is Earth's surface) from various studies: QM1 (*Widmer et al.*, 1991), SL8 (*Anderson and Hart*, 1978), QLM9 (*Lawrence and Wysession*, 2006), and QI6 (*Durek and Ekström*, 1996). Figure from *Romanowicz and Mitchell* (2007).

The  $ScS$  and  $ScS_2$  phases are frequently used seismic phases in studies of  $Q$  in the deep mantle. They propagate nearly vertically through the mantle and reflect off the outer core and Earth's surface without energy loss. For short epicentral distances,  $ScS$  and  $ScS_2$  have nearly identical propagation paths except that  $ScS_2$  has an extra bounce. The ratio of the  $ScS$  and  $ScS_2$  amplitudes, recorded by the same seismic instrument and for the same earthquake, is a reliable measure of wave attenuation. It is unaffected by uncertainties of the initial signal strength (the excitation by the earthquake) and signal amplification by seismic instrumentation. The study by *Kovach and Anderson* (1964) was the first to determine  $Q$  from spectral ratios of multiple  $ScS$

waves, finding an average  $Q$  of 600 for the entire mantle. *Jordan and Sipkin* (1977) developed a phase equalization and phase-stacking algorithm to document large lateral variations in  $Q$ . Multiple ScS studies in the Pacific have documented  $Q$  of 139-161 beneath the Lau Basin (*Flanagan and Wiens*, 1998),  $Q$  of 160 beneath the Sea of Japan (*Nakanishi*, 1979), an unusually high  $Q$  of 366 below the Ontong-Java Plateau (*Gomer and Okal*, 2003), and an unusually low  $Q$  of 70-80 in the South Pacific Superswell (*Suetsugu*, 2001).

This thesis follows up on the recent study of  $ScS_2/ScS$  ratios by *Kanamori and Rivera* (2015), who documented a remarkably high value of 1400 for the average  $Q$  in the mantle beneath Global Seismic Network station AFI (Afiamalu, Samoa). This is among the high values for  $Q$  ever reported and implies that attenuation throughout the mantle beneath Samoa is extremely low. Low attenuation is in stark contrast to high wave attenuation in the upper mantle beneath the Lau Basin (*Flanagan and Wiens*, 1998) and the presence of a broad low shear wave zone in the lower mantle beneath the southwestern Pacific (e.g., *Ritsema et al.*, 1999) within several hundreds kilometers. These latter observations suggest that the temperature in the upper and lower mantle is elevated. We explore *Kanamori and Rivera's* (2015) observation further by expanding the analysis with additional ScS multiples and surface reflections, by analyzing data from seismic station EUAT (from a temporary regional network in the Tonga region) close to AFI, and by modeling complete waveforms with synthetics rather than peak-to-peak amplitudes.

## 2. Methods

### 2.1 ScS and sScS ray geometry

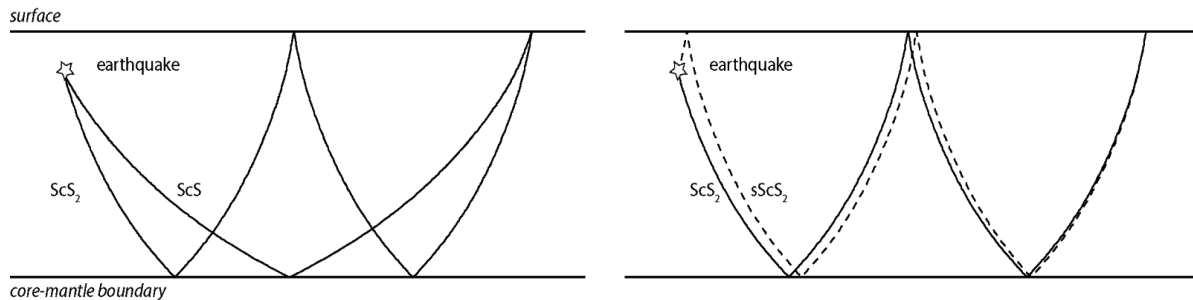


*Figure 2.* (left) Ray paths of ScS and sScS for an earthquake at 500 km depth. ScS bounces off the core once. ScS<sub>2</sub> reflects off the surface once and off the core twice. (right) Ray paths of ScS<sub>2</sub> and sScS<sub>2</sub>. The surface reflection sScS<sub>2</sub> first propagates upward, reflecting off the surface before following a path similar to ScS<sub>2</sub>.

In this study we estimate attenuation from the amplitudes of six shear-wave reflections of the core. The phases ScS, ScS<sub>2</sub> and ScS<sub>3</sub> propagate downward from the earthquake and reflect once,

twice and three times off the core, respectively. The phases  $sScS$ ,  $sScS_2$  and  $sScS_3$  are similar to  $ScS$ ,  $ScS_2$  and  $ScS_3$  but propagate upward from the source and reflect off Earth's surface first (Figure 2). Hence, these surface reflections propagate longer paths through the upper mantle than the initially downward  $ScS$  phases.

Figure 3 shows the transverse-component seismogram (a ground motion record of primarily shear wave motions) of a deep earthquake in Tonga (see section 3.1) at seismic station AFI used in our analysis. This seismogram includes  $ScS$ ,  $sScS$ ,  $ScS_2$ ,  $sScS_2$ ,  $ScS_3$ , and  $sScS_3$  high above noise level when lowpass filtered at  $T > 25$  s. The time between  $ScS_2$  and  $ScS$  and between  $ScS_3$  and  $ScS_2$  is the two-way traveltimes (of about 935 s) of a shear wave across the mantle. The time between  $sScS$  and  $ScS$  and between  $sScS_2$  and  $ScS_2$  (of about 230 s) is roughly the two-way traveltimes of a shear wave between the earthquake (at 533 km depth) and Earth's surface. The systematic amplitude decay is caused by geometric spreading and attenuation.

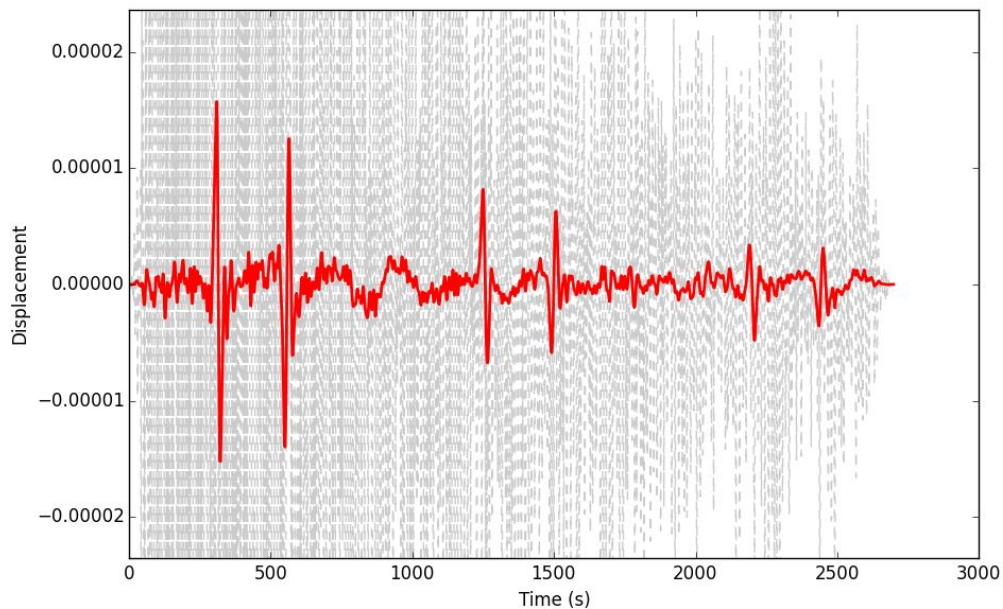
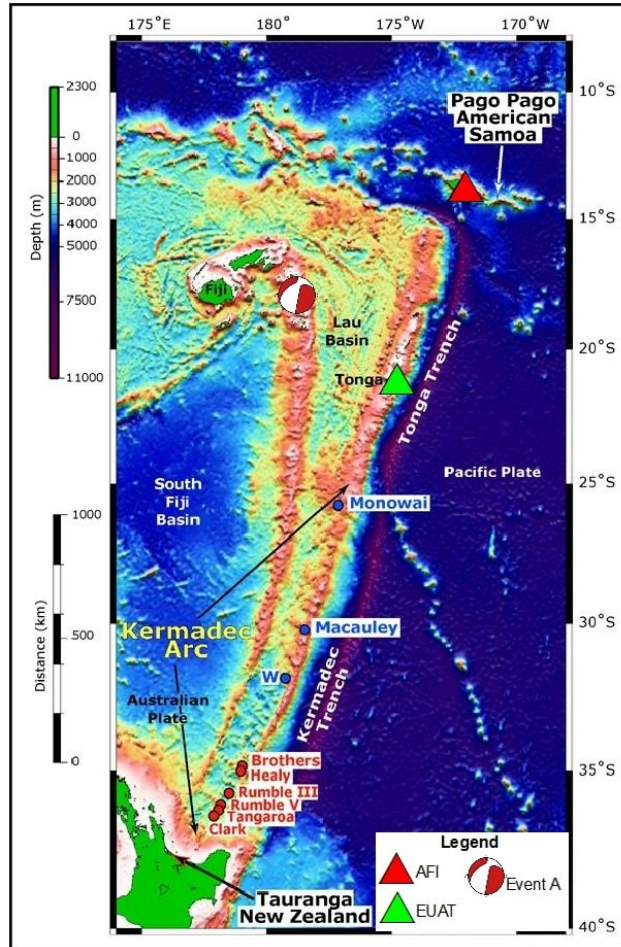


Figure 3. Transverse-component (motions orthogonal to the plane of propagation) seismogram at global seismic network station AFI (Afiamalu, Samoa) generated by the March 9, 1994 Tonga earthquake. The seismograms (in red) is lowpass filtered at  $T > 25$  s. The six high amplitude signals are (from left to right):  $ScS$ ,  $sScS$ ,  $ScS_2$ ,  $sScS_2$ ,  $ScS_3$ ,  $sScS_3$ . The unfiltered seismogram is shown in grey.

The recorded and computed (i.e., synthetic) seismogram for a standard seismic model, such as the Preliminary Reference Earth Model or PREM (Dziewonski and Anderson, 1981), have three fundamental differences. First, the  $ScS_2$  (and  $sScS_2$ ) and  $ScS_3$  (and  $sScS_3$ ) reflections arrive later than in the PREM synthetic. Second, the amplitude decay of the core reflections is smaller in the recorded than the PREM synthetic. Third, the recorded  $ScS_2$  and  $ScS_3$  signals have a higher frequency content than the same signals in the PREM synthetic. The traveltimes differences indicate that, on average, the shear wave speed in the mantle between the Tonga earthquake and

AFI is lower than in PREM. The small amplitude decay and the relatively high-frequency content of  $ScS_2$  and  $ScS_3$  indicate that shear wave attenuation in the mantle below AFI is relatively low.

## 2.2 Shear wave recordings



*Figure 4.* Bathymetry map of the study area. Triangles indicate the location of stations AFI and EUAT. The “beachball” indicates the location and source mechanism of the March 9, 1994 earthquake near Tonga. Also shown are the Tonga and Kermadec Trenches, where active subduction is occurring. Image courtesy of NOAA.

We analyze event A using horizontal-component seismograms from station AFI to the northeast and station EUAT to the southeast of event A (Figure 4) at epicentral distances of  $\Delta = 7.56^\circ$  and  $\Delta = 4.72^\circ$ , respectively. We download the data as SAC files from the IRIS Data Management Center archives using WILBER-III ([www.iris.edu](http://www.iris.edu)). The data are corrected for the instrument response and converted to ground velocity. We project the horizontal-component seismograms

into a transverse-component waveform to isolate wave polarization in the transverse direction, i.e. the direction orthogonal to the source-receiver propagation direction. By filtering using a lowpass Butterworth filter with a corner frequency of 25 mHz over 2 passes, waveform complexity due to unmodeled rupture directivity and crust and mantle heterogeneity in the Tonga subduction zone is suppressed. Finally, we taper the waveforms using  $\sin^2$  and  $\cos^2$  tapers.

### 2.3 Amplitude ratios.

We estimate the shear wave quality factors  $Q$  in the mantle from the amplitudes of ScS and its multiples which are recorded above noise level for event A. We determine amplitude anomalies from the cross-correlation coefficients of recorded and computed (i.e. synthetic) waveforms. The synthetic waveforms have been computed using the AxiSEM method (*Nissen-Meyer et al.*, 2014) for the PREM wavespeed structure and the hypocentral location and moment tensor source parameters reported in the Global CMT catalog. The AxiSEM synthetics include amplitude variations due to variable shear wave radiation from the source and amplitude decay due to geometric spreading and attenuation. We modify the attenuation structure as discussed in section 2.4. We convolve the synthetics with the source time function determined by *Vallée et al.* (2011) to include the effects of rupture finiteness.

We determine two ratios,  $A_1$  and  $A_2$ , between the recorded,  $d(t)$ , and synthetic,  $s(t)$ , waveforms by minimizing the integrated squared difference between  $d(t)$  and  $s(t)$  in a 80-s wide cross-correlation window  $W$  around the phases of interest. The value  $A_1$  minimizes

$$\int_W [d(t) - A_1 s(t)]^2 dt \quad (3a)$$

and  $A_2$  minimizes

$$\int_W [A_2^{-1} d(t) - s(t)]^2 dt \quad (3b)$$

$A_1$  and  $A_2$  can be computed from the crosscorrelation and autocorrelation functions (*Ritsema and Van Heijst*, 2002):

$$A_1 = \max(d^*s) / s^*s \quad (4a)$$

and

$$A_2 = d^*d / \max(d^*s) \quad (4b)$$

where ‘\*’ denotes correlation. If  $d$  and  $s$  were identical,  $A = A_1 = A_2$  is simply a scaling factor. Since  $d$  and  $s$  are always different due to noise and simplifications in the modeling, we define the amplitude ratio  $A$  between  $d(t)$  and  $s(t)$  as

$$A = \frac{A_1 + A_2}{2} \quad (5)$$

and the uncertainty  $E$  in the amplitude  $A$  by

$$E = \left| \frac{A_1 - A_2}{2} \right| \quad (6)$$

## 2.4 Model parameters and selection

We parameterize the  $Q$  structure using two free parameters.  $Q_{UM}$  and  $Q_{LM}$  are the quality factors for the upper mantle (0-670 km) and lower mantle (670-2891 km), respectively. We do not consider lateral variations of  $Q_{UM}$  and  $Q_{LM}$  but let differences in the estimates for different stations inform us on possible geographic variations. In the modeling we vary  $Q_{UM}$  and  $Q_{LM}$  between 50 and 2000, and calculate a data bank of synthetics in which  $Q_{UM}$  and  $Q_{LM}$  have discrete values of 50, 80, 100, 200, 500, 800, 1000, and 2000. This range captures the variability of ScS amplitude and waveforms due to attenuation in the mantle.

We determine the goodness of fit for a given model of attenuation, determined by  $Q_{UM}$  and  $Q_{LM}$ , from the least-squares mismatch between the inferred amplitude factors  $A$  and their uncertainties  $E$  for each of the six phases (Figure 5):

$$\chi^2 = \sum_{i=1}^6 \frac{(A_i - \mu)^2}{(\mu E_i)^2} \quad (7)$$

where  $i$  is the index integer for each of the six ScS signals.  $A$  (equation 5) and  $E$  (equation 6) are the scaling factors and uncertainties computed from cross correlation (see Figure 5), and  $\mu$  is the mean of the six misfit values for each ScS signal. The optimal combination of  $Q_{UM}$  and  $Q_{LM}$  produces the most consistent set of amplitudes  $A_i$  (apart from a common amplitude factor  $\mu$ ) and the lowest value for  $\chi^2$ . By plotting  $\chi^2$  as a function of  $Q_{UM}$  and  $Q_{LM}$  we evaluate the resolution of  $Q_{UM}$  and  $Q_{LM}$ , leaving a rigorous statistical analysis as future work.

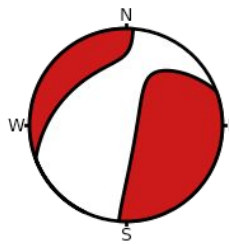
## 3. Event A: March 9, 1994, $M_w$ 7.6, $H = 534$ km, Samoa Islands

We have limited our analysis to a deep earthquake that occurred on 9 March 1994 beneath the Samoa Islands (Table 1). This earthquake, which we call event A, had a moment magnitude



( $M_w$ ) of 7.6 and a vertical dip-slip double-couple mechanism according to the Global CMT catalog (Dziewonski *et al.*, 1981; www.globalcmt.org). A double-couple source with a vertical dip slip mechanism is effective in radiating high-amplitude shear waves, such as ScS and sScS, in the up and downward direction. The large event depth of 533.9 km ensures that the ScS and sScS phases and their multiples are separated by at least 230 seconds. This simplified measuring amplitude ratios. Moreover, event A (like most other deep earthquakes) had a relatively short rupture duration of 16 s (e.g., Goes and Ritsema, 1995) and produced waveforms without strong directivity that could complicate wave analysis.

Table 1. Event A source parameters and stereonet diagram of the full moment tensor

Date: 1994/ 3/ 9	Centroid Time: 23:28:17.7 GMT			
Lat = -17.69	Lon = -178.11			
Depth = 567.8	Half duration = 16.0			
Centroid time minus hypocenter time: 10.0				
$M_w = 7.6$	$m_b = 6.6$		$M_s = 0.0$	Scalar Moment = $3.07e+27$
Nodal plane 2: strike = 250	dip = 27		slip = -30	
Nodal plane 1: strike = 7	dip = 77		slip = -114	

## 4. Results

### 4.1 Station AFI

Figure 5 illustrates the measurements of A and E for ScS, sScS, ScS<sub>2</sub>, sScS<sub>2</sub>, ScS<sub>3</sub>, and sScS<sub>3</sub> for our preferred two-layer model of Q:  $Q_{UM} = 2000$  and  $Q_{LM} = 2000$ . The top panel shows the recorded and PREM seismogram including ScS, sScS, ScS<sub>2</sub>, sScS<sub>2</sub>, ScS<sub>3</sub>, and sScS<sub>3</sub> (see also Figure 3). The six lower panels show the initial PREM and optimal match between recorded and synthetic waveforms after alignment and scaling. The time shifts  $\Delta T$  have been applied to obtain highest waveform correlation.  $\Delta T$  is positive for each phase, indicating that the shear velocity of the mantle between event A and AFI is, on average, lower than in PREM. Since ScS<sub>3</sub> and sScS<sub>3</sub> have the longest propagation paths, they are delayed most with respect to the predicted PREM arrival times. All scaling factors A are lower than 1, so the amplitudes of all seismic phases are overestimated by the PREM synthetic, presumably because the seismic moment reported in the Global CMT catalog is too high. The relatively high errors E for ScS<sub>3</sub> and sScS<sub>3</sub> indicates that the multiple ScS propagation is complicated by the heterogeneous crust and upper mantle in the region. Nevertheless, the amplitude scaling factors A for all six phases agree within error E with the synthetics computed for the model of Q used in this simulation.

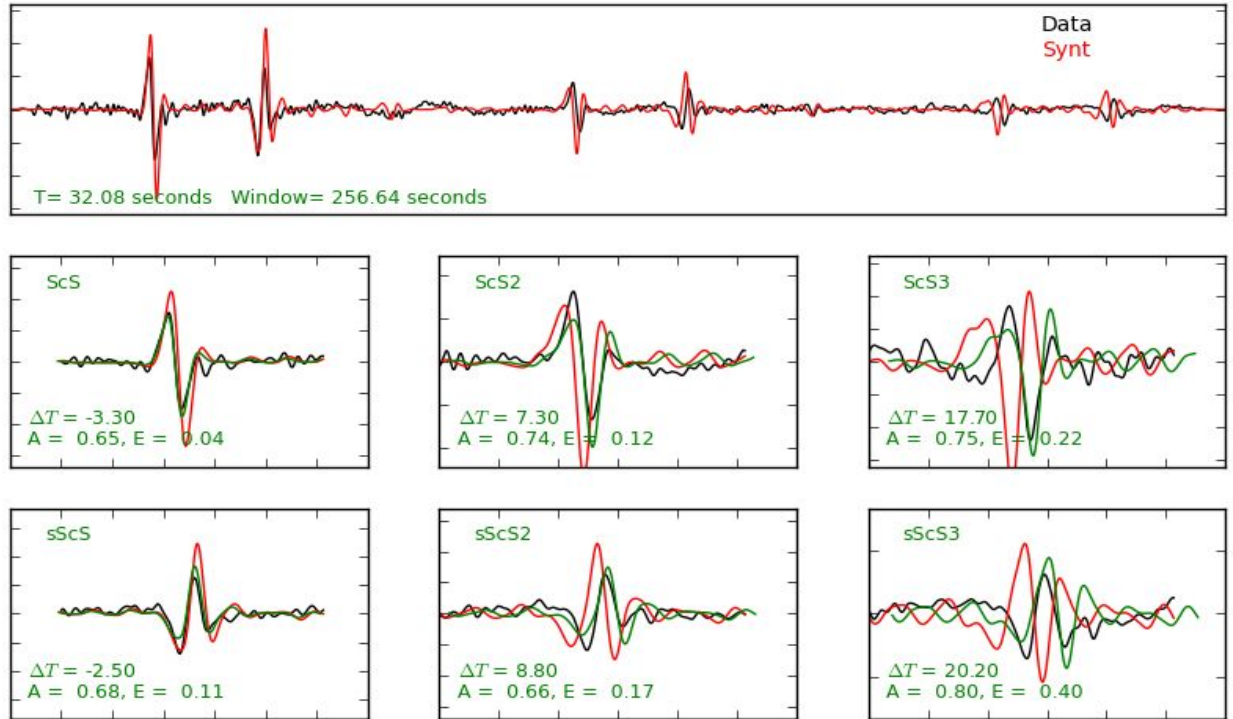


Figure 5. Illustration of the measurements of A and E. The top panel show the (in black) recorded and (in red) PREM transverse component seismogram of event A at AFI. The lower six panels show windows around (upper row) ScS, ScS<sub>2</sub>, ScS<sub>3</sub>, (lower row) sScS, sScS<sub>2</sub>, sScS<sub>3</sub>. The recorded signals are in black, the PREM synthetic is in red, and the synthetic (after alignment  $\Delta T$ ) for  $Q_{UM} = 2000$  and  $Q_{LM} = 2000$  is in green. The estimated values for A and E are indicated in the lower-left corner of each panel.

Figure 6 shows  $\chi^2$  as a function of  $Q_{UM}$  and  $Q_{LM}$  for all 6 signals combined. The misfit  $\chi^2 = 6.233$  for the best-fitting model when  $Q_{UM} = Q_{LM} = 2000$  ( $\log_{10} Q = 3.3$ ) which means that the uncertainty E in the six amplitude scaling factors is similar to the variation of the amplitude factor A from the mean value. That is, the amplitudes are fit perfectly within uncertainty.  $Q_{UM} = Q_{LM} = 2000$  are the highest Q values that we have explored in our modeling. For these values, attenuation is undetectable in the modeled long-period ScS signals. The internal consistency of the amplitude scaling factors A for the six ScS phases increases, with exception to small values of  $Q_{LM}$ , as the values for both  $Q_{UM}$  and  $Q_{LM}$  increase. The scaling factors A are sensitive primarily to  $Q_{LM}$  because all ScS phases propagate the longest paths through the lower mantle and thus are influenced most by attenuation parameters in the lower mantle.

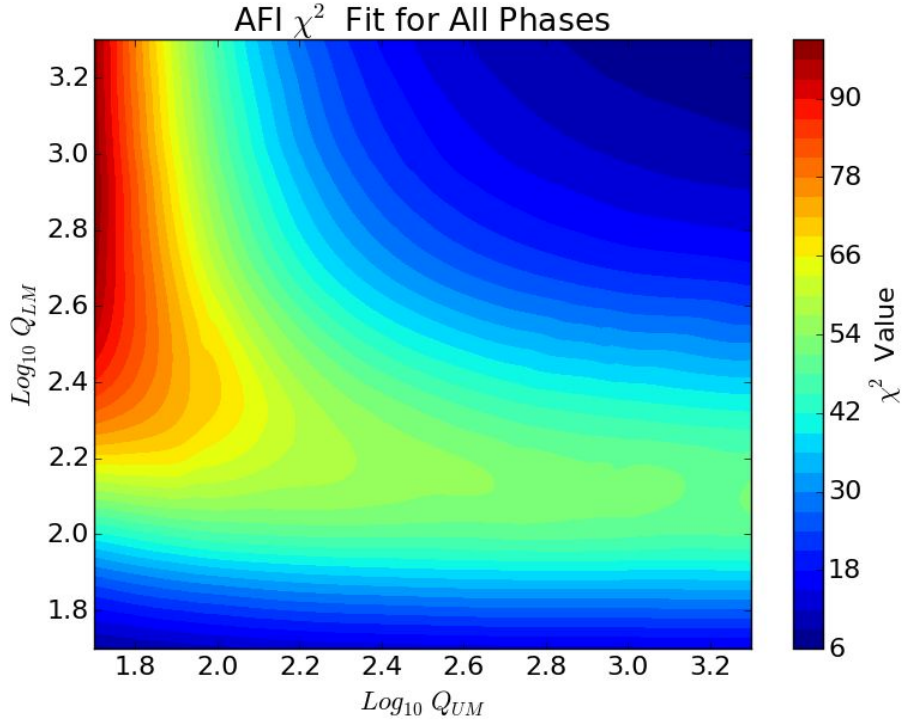


Figure 6.  $\chi^2$  as a function of  $\log_{10} Q_{UM}$  (x-axis) and  $\log_{10} Q_{LM}$  (y-axis) computed for station AFI based on the amplitude A and error E measurement for ScS, sScS, ScS<sub>2</sub>, sScS<sub>2</sub>, ScS<sub>3</sub>, and sScS<sub>3</sub>. The contour colors indicate  $\chi^2$ . The coolest colours represent the best fit.

The low values of  $\chi^2$  obtained when  $Q_{LM} < 100$  are due to our choice to include in  $\chi^2$  (equation 7) only a term that quantifies the consistency of the scaling factors A for each phase and to exclude the fit between the recorded and synthetic signals. As shown in Figure 5, the scaling factors A have similar values for all phases when  $Q_{UM} = Q_{LM} = 2000$ . The similarity of A results in the minimum in  $\chi^2$ . When  $Q_{LM} < 100$ , the spread of A is relatively large but the significant errors E result in low values for  $\chi^2$  because  $(\mu E_i)^2$  appears in the denominator of equation (7). By inspection, we have verified that an attenuation structure with  $Q_{LM} < 100$  predicts ScS signals that are much broader than the signals in the recordings. As E is a measure of waveform misfit (see equations 3a and 3b) we can infer optimal values for  $Q_{UM}$  and  $Q_{LM}$  also from the minimum value of E and, in fact, let E contribute to  $\chi^2$  as in equation (8).

$$\chi^2 = \sum_{i=1}^6 \frac{(A_i - \mu)^2}{(\mu E_i)^2} + \lambda \sum_{i=1}^6 E_i^2 \quad (8)$$

where  $\lambda$  is a weight factor that determines the contribution of waveform misfit (i.e., the second term) to  $\chi^2$ . Figure 7 displays E and A as a function of  $Q_{UM}$  and  $Q_{LM}$ . E is relatively high for  $Q_{UM} < 100$  which demonstrates that a misfit function  $\chi^2$  that includes a term representing waveform

fit, such as the 2<sup>nd</sup> term in equation (8), would have a unique minimum. Follow-up work must therefore address a form of  $\chi^2$  that incorporates a measure of waveform fit.

The decrease of  $\chi^2$  by a factor of 10 when  $Q_{UM}$  is increased from 100 to 2000 and  $Q_{LM} = 2000$  (Figure 6) indicates that the amplitude measurements have some sensitivity to  $Q_{UM}$ . Figure 7 shows that this resolving power is provided by the sScS signal since E computed for sScS is smallest for largest values of  $Q_{UM}$ . E does not exhibit a clear minimum for  $Q_{UM}$  for ScS, a phase that has only one propagation segment in the upper mantle. However, E determined for just sScS has a defined minimum in both  $Q_{UM}$  and  $Q_{LM}$ . That sScS is more sensitive to  $Q_{UM}$  than ScS is not surprising since sScS propagates two extra legs through the upper mantle (see Figure 2). We find a similar sensitivity to  $Q_{UM}$  for sScS<sub>2</sub> and sScS<sub>3</sub> but do not illustrate it here.

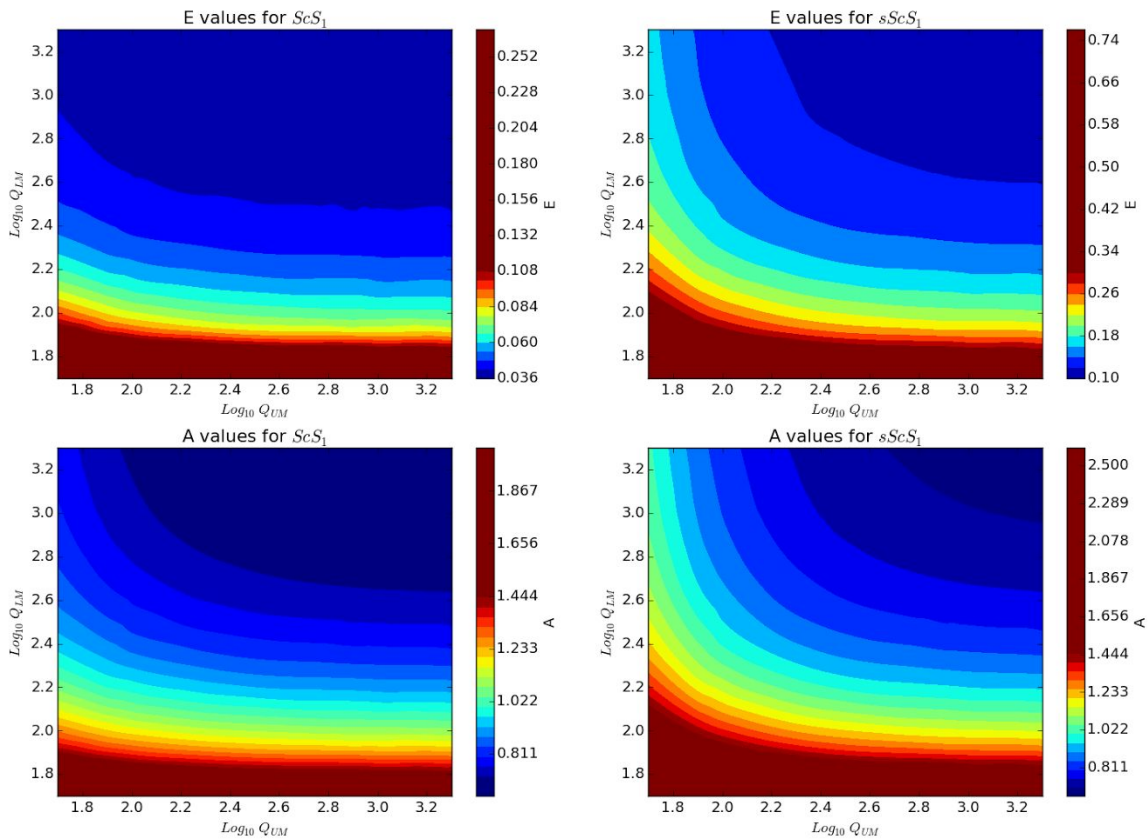


Figure 7. Measures of E (top row) and A (bottom row) as a function of  $\log_{10}(Q_{UM})$  and  $\log_{10}(Q_{LM})$ . The left column is measurements for phase ScS, the right column is measurements for sScS. Note that sScS is more sensitive to  $Q_{UM}$  than ScS. The color spectra represent the change in A and E. Note the saturation at the intermediate values.

Whether the attenuation model [ $Q_{UM} = 2000$ ;  $Q_{LM} = 2000$ ] is better than the model [ $Q_{UM} = 200$ ;  $Q_{LM} = 2000$ ] must be evaluated by a more complete waveform analysis that includes an investigation of the velocity structure and the source parameters on the waveforms. Here, we

assume the Global CMT moment tensor solution for sScS and ScS radiation (i.e. initial amplitudes) and we ignore the effect of local heterogeneity on the ScS waveforms. An analysis of synthetics, based on different moment tensor solutions and more complicated wave speed structures, is beyond the scope of this thesis but must be addressed in future research.

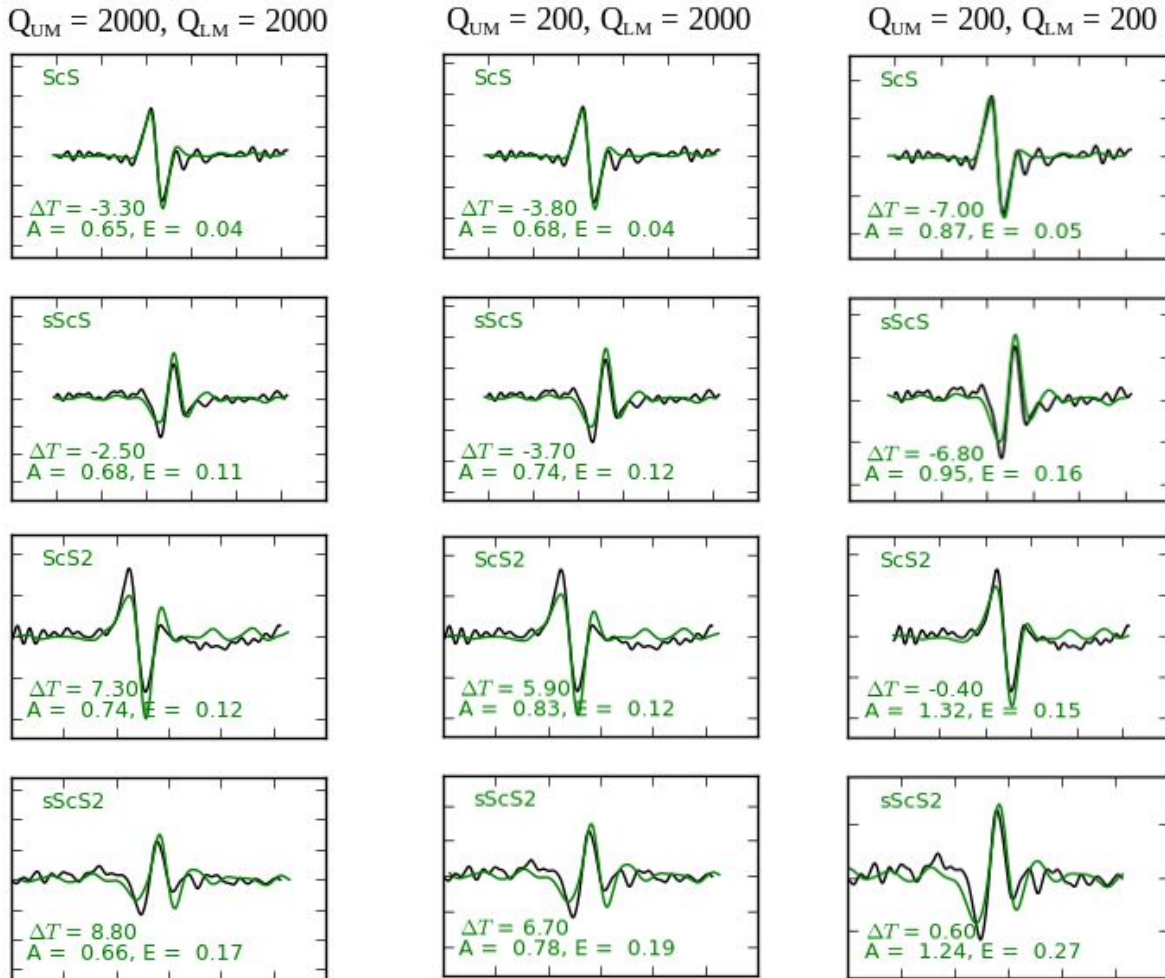


Figure 8. Waveform fits to (top row) ScS, (2<sup>nd</sup> row) sScS, (3<sup>rd</sup> row) ScS<sub>2</sub> and (bottom row) sScS<sub>2</sub> for Q models defined by (left) [ $Q_{UM} = 2000; Q_{LM} = 2000$ ], (middle) [ $Q_{UM} = 200; Q_{LM} = 2000$ ], and (right) [ $Q_{UM} = 200; Q_{LM} = 200$ ]. The recorded waveforms are in black, the synthetic waveforms are in green.

Figure 8 compares the waveform fits for several attenuation models to illustrate the variation of waveform fit as a function of attenuation. Model [ $Q_{UM} = 2000; Q_{LM} = 2000$ ] results in the lowest value of  $\chi^2$  since the scaling factors A for the ScS signal, which range from 0.65 to 0.74, are most consistent. As discussed, model [ $Q_{UM} = 200; Q_{LM} = 2000$ ] has a slightly higher misfit  $\chi^2$  given the slightly more inconsistent scaling factors. Model [ $Q_{UM} = 200; Q_{LM} = 200$ ], which is more representative of the average attenuation structure of the mantle, yields inconsistent scaling factors: they vary between  $0.87 \pm 0.05$  for ScS to  $1.32 \pm 0.15$  for ScS<sub>2</sub>. The high value for ScS<sub>2</sub> indicates that synthetic waveform computed for the attenuation model underpredicts the recorded



amplitude of  $ScS_2$ , and, therefore, that attenuation is too strong. The waveform fits, expressed by  $E$ , are similar for models  $[Q_{UM} = 2000; Q_{LM} = 2000]$  and  $[Q_{UM} = 200; Q_{LM} = 2000]$ , ranging from 0.04 to 0.19.  $E$  is significantly higher for model  $[Q_{UM} = 200; Q_{LM} = 200]$  because the relatively high attenuation results in strong broadening of the signals in the synthetics that is not seen in the recordings.

#### 4.2 Station EUAT

Waveform data from station EUAT, from a temporary regional seismic network in the region, allows us to evaluate whether the low attenuation observed at AFI is a regional phenomena. EUAT is located to the south of AFI (see Figure 4) and the surface reflection of  $ScS_2$  and  $ScS_3$  reflect off the surface within the Lau Basin. Figure 9 shows  $\chi^2$  as a function of  $Q_{UM}$  and  $Q_{LM}$  akin to Figure 6. Like AFI, we resolve the lowest value for  $\chi^2$  ( $\chi^2 = 4.2126$ ) when  $Q_{LM} = 2000$ . However, in contrast to AFI, the minimum value is obtained for  $Q_{UM} = 100$ .

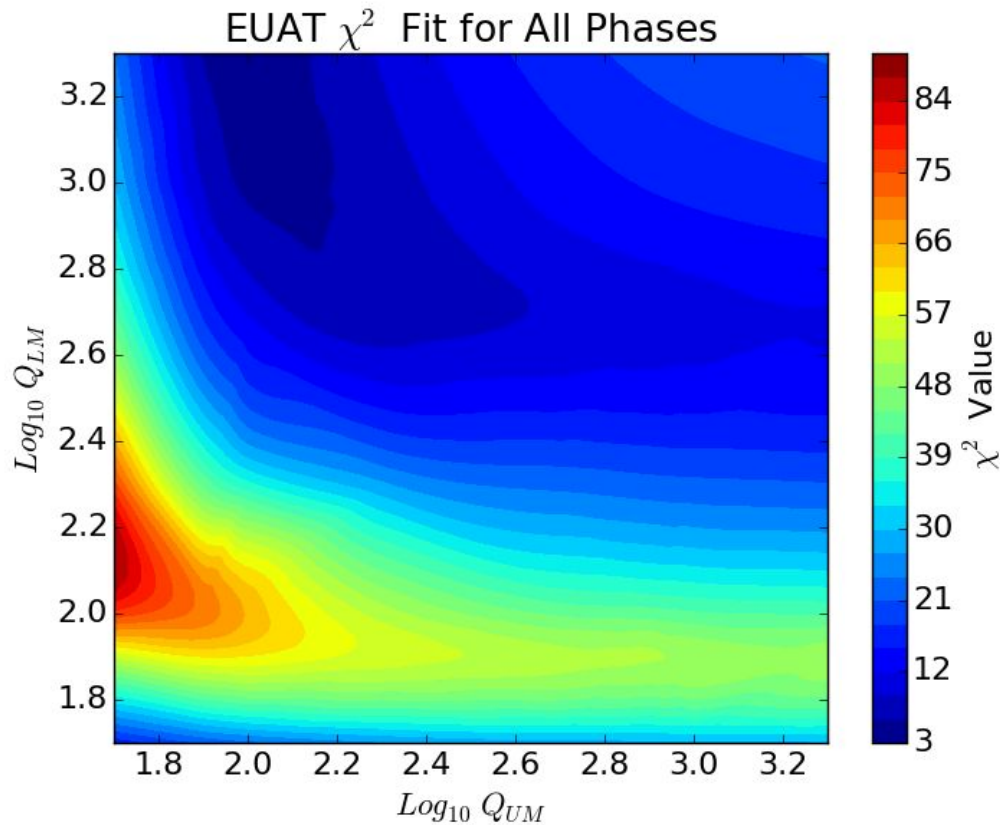


Figure 9.  $\chi^2$  as a function of  $\log_{10} Q_{UM}$  (x-axis) and  $\log_{10} Q_{LM}$  (y-axis) computed for station EUAT based on the amplitude  $A$  and error  $E$  measurement for  $ScS$ ,  $sScS$ ,  $ScS_2$ ,  $sScS_2$ ,  $ScS_3$ , and  $sScS_3$ . The contour colors indicate  $\chi^2$ . The coolest colours represent the best fit.

Figure 10 addresses the resolution of  $Q_{UM}$  by comparing  $A$ ,  $E$  and waveform fits for attenuation models  $[Q_{UM} = 2000; Q_{LM} = 2000]$  and  $[Q_{UM} = 100; Q_{LM} = 2000]$ . The smaller variation in the

scaling factors  $A$  of 0.74-0.83 for  $Q_{UM} = 100$ , compared to 0.54-0.71 for  $Q_{UM} = 2000$ , results in the of  $\chi^2$  for  $Q_{UM} = 100$ . This variation is slightly larger than the standard errors  $E$ , but the robustness must be evaluated by experimenting with the effect of the moment tensor and velocity structure on synthetic waveforms.

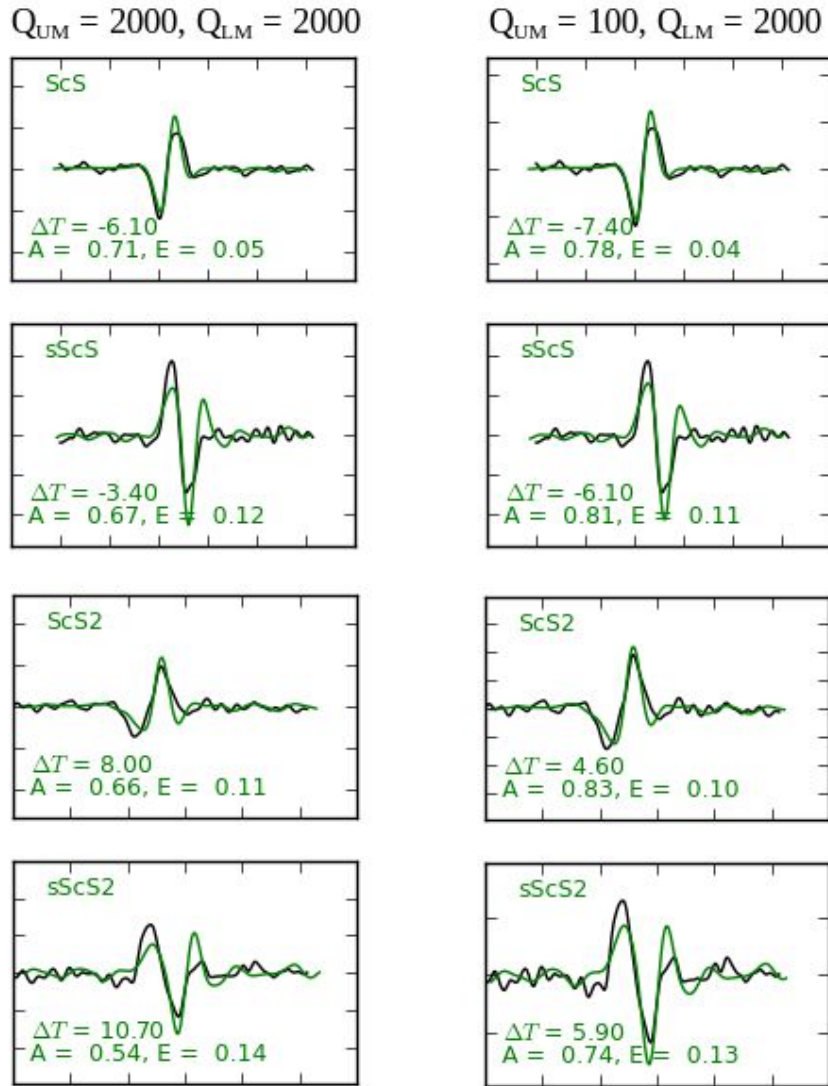


Figure 10. Waveform fits to (top row) ScS, (2<sup>nd</sup> row) sScS, (3<sup>rd</sup> row) ScS<sub>2</sub> and (bottom row) sScS<sub>2</sub> for  $Q$  models defined by (left) [ $Q_{UM} = 2000; Q_{LM} = 2000$ ] and (left) [ $Q_{UM} = 100; Q_{LM} = 200$ ]. The recorded waveforms are in black, the synthetic waveforms are in green.

For the same reason as with station AFI, the minimization of  $E$  as a function of  $Q_{UM}$  and  $Q_{LM}$  is useful in identifying for which  $Q_{UM}$  and  $Q_{LM}$  the synthetic phase requires the least scaling to match the recorded phase. Figure 11 shows  $E$  as a function of  $Q_{UM}$  and  $Q_{LM}$  for ScS<sub>1</sub> and sScS<sub>1</sub>.

For both phases, E is minimized at  $Q_{UM} = 50$ ,  $Q_{LM} = 200$ . Again, the addition of an extra travel path through the upper mantle increases the resolution of the fit against  $Q_{UM}$ , indicating the waveform is sensitive to the additional attenuation incurred in the upper mantle during  $sScS_1$ . Unlike for station AFI, which identified the same Q parameters producing the lowest error and lowest  $\chi^2$  values, the results for EUAT identify a discrepancy between the Q parameters minimizing E and  $\chi^2$ , with lower values of both  $Q_{UM}$  and  $Q_{LM}$  producing the smallest E. As Figure 10 shows, the amplitude scaling factors A are all smaller than 1, meaning that the PREM synthetic is overestimating the seismic moment and all of the recorded waveform amplitudes must be increased to match the synthetic.  $Q_{UM} = 50$ ,  $Q_{LM} = 200$ , then, is the synthetic that requires the least scaling to match the  $ScS_1$  and  $sScS_1$  phases of the recorded waveform, but for all six phases our  $\chi^2$  test indicates this synthetic is not producing the most consistent values of A, and is therefore not the best fitting model for the loss in energy across all six phase arrivals.

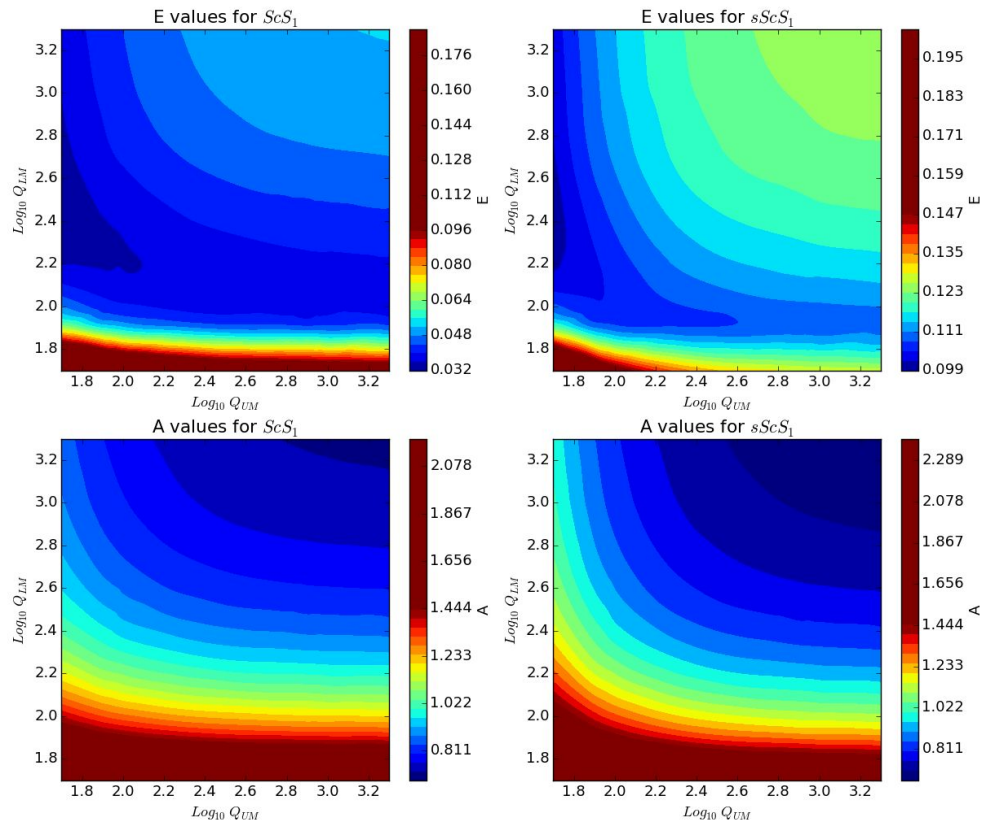


Figure 11. Measures of E (top row) and A (bottom row) as a function of  $\log_{10}(Q_{UM})$  and  $\log_{10}(Q_{LM})$ . The left column is measurements for phase  $ScS$ , the right column is measurements for  $sScS$ .

## 5. Discussion

The seismic quality factor Q is a measure of seismic attenuation and quantifies energy lost per wave cycle, recorded by the decay of the amplitude of seismic waves. A recent study by



*Kanamori and Rivera* (2015) shows that shear-wave propagation beneath Samoa is extremely low. In this thesis, we have followed up on this paper by modeling ScS wave amplitudes using a new approach. We have analyzed waveform recordings of near-vertical ScS waves from a deep earthquake in the Tonga region at station within several hundred kilometers distance. By analyzing the surface reflected sScS, sScS<sub>2</sub> and sScS<sub>3</sub> phases generated by deep earthquakes we have attempted to constrain the quality factor  $Q_{UM}$  in the upper mantle independently from the quality factor  $Q_{LM}$  in the lower mantle. Further, our measurement of wave amplitudes are obtained from the correlation of recorded and synthesized waveform. Waveform correlation functions provide a measurement of the wave amplitudes on the basis of the entire waveform in contrast to the peak-to-peak amplitude, which is essentially a measurement at a single time sample. We quantified the goodness of fit  $\chi^2$  from the consistency of six scaling factors that optimize the match between recorded and computed amplitudes of ScS, ScS<sub>2</sub>, ScS<sub>3</sub>, sScS, sScS<sub>2</sub>, and sScS<sub>3</sub>. We have not included in  $\chi^2$  a measure of waveform fit that expresses how well signal broadening due to attenuation is reproduced by the synthetic waveform. Our preliminary analysis indicates that a misfit function fit  $\chi^2$  with terms representing the consistency of amplitude scaling and waveform misfit (i.e. equation 8) may provide a unique misfit minimum.

We confirm *Kanamori and Rivera's* (2015) observation that attenuation is anomalously low beneath seismic station AFI on Samoa. We find similarly low attenuation beneath seismic station EUAT further to the south. There is a hint in our data that the quality factor  $Q_{UM}$  for the upper mantle is lower for EUAT, but a rigorous statistical and seismological analysis is required to determine the robustness of this observation. New research should evaluate the effects of uncertainties in the moment tensor that determines the initial amplitudes of ScS (and its multiples) and sScS (and its multiples). Further, the effect of wave speed heterogeneity in the Tonga subduction zone may be important.

The Samoan islands, situated nearby the convergent boundary of the Pacific and Tonga plates (Figure 4), are traditionally considered a hotspot trail associated with a deep mantle plume, as evidenced by the linear age progression of the islands (*Hart et al.*, 2004; *Koppers et al.*, 2008). Global images (e.g., *Ritsema et al.*, 1999) reveal low wave speed structure in the lower mantle beneath the Pacific. If the geologic and seismic observations point to an anomalously hot mantle beneath Samoa it is surprising that the quality factor  $Q$  for the region is high. The high  $Q$  that we, and *Rivera and Kanamori* (2015) observe, is also in disagreement with the global  $Q$  model presented by *Gung and Romanowicz* (2004). *Kanamori and Rivera* (2015) propose a laterally heterogeneous structure of a low-velocity core surrounded by a high-velocity sheath that enhance S-wave amplitudes by focusing, resulting in very high  $Q$  observations.

Although we must conduct new analyses to determine the resolution of  $Q_{UM}$  independently from  $Q_{LM}$ , we speculate that higher attenuation in the upper mantle (i.e. a lower value for  $Q_{UM}$ ) for

EUAT has a geologic origin. Multiple ScS waves propagating to EUAT reflect off the surface beneath the Lau Basin. Wave attenuation in the upper mantle beneath the Lau Basin is expected, and observed, to be high ( $Q = 139\text{-}161$  according to *Flanagan and Wiens, 1998*) due to back-arc spreading and active volcanism. The ScS waves between event A and AFI may not sample the Lau Basin but instead propagate predominantly through the cold slabs of subducted lithosphere that do not attenuate shear waves. If the difference in  $Q_{\text{UM}}$  and  $Q_{\text{LM}}$  can indeed be robustly determined, the analytical approach presented in thesis may be useful to document the scale of  $Q$  variations in both the upper mantle and lower mantle from ScS waves in subduction zones where regional seismic networks have been deployed.

## 6. Conclusions

This study presents further evidence of remarkably high  $Q$  values in the mantle beneath the Samoan islands. By computing cross-correlation coefficients of recorded and synthetic waveforms and calculating the synthetic waveform that produces the most consistent amplitude scaling ratios, we estimate that, on average,  $Q = 2000$ , in the lower beneath seismic stations AFI and EUAT. Our data also suggest that  $Q$  is much lower in the upper mantle beneath EUAT, albeit that rigorous follow-up analysis is necessary to confirm this observation. These results are in agreement with the study by *Kanamori and Rivera (2015)*, and they are surprising given the hotspot setting and location of Samoa above a broad low shear-wave velocity anomaly in the lower mantle.

## 7. References Cited

- Anderson, D. L., & Hart R. S. (1978).  $Q$  of the Earth. *Journal of Geophysical Research: Solid Earth*, 83(B12), 5869–5882.
- Benz, H. M., Frankel, A., & Boore, D. M. (1997). Regional Lg attenuation for the continental United States. *Bulletin of the Seismological Society of America*, 87(3), 606-619.
- Dalton, C. A., & Ekström, G. (2006). Global models of surface wave attenuation. *Journal of Geophysical Research: Solid Earth (1978–2012)*, 111(B5).
- De Souza, J. L., & Mitchell, B. J. (1999). Lg coda  $Q$  variations across South America and their relation to crustal evolution. In *Q of the Earth: Global, Regional, and Laboratory Studies* (pp. 587-612). Birkhäuser Basel.
- Durek, J. J., & Ekström, G. (1996). A radial model of anelasticity consistent with long-period surface-wave attenuation. *Bulletin of the Seismological Society of America*, 86(1A), 144-158.
- Dziewonski, A. M., & Anderson, D. L. (1981). Preliminary reference Earth model. *Physics of the earth and planetary interiors*, 25(4), 297-356.

- Faul, U. H., & Jackson, I. (2005). The seismological signature of temperature and grain size variations in the upper mantle. *Earth and Planetary Science Letters*, 234(1), 119-134.
- Flanagan, M. P., & Wiens, D. A. (1998). Attenuation of broadband P and S waves in Tonga: Observations of frequency dependent Q. *Pure appl. Geophys.*, 153, 345-375
- Goes, S., & Ritsema, J. (1995). A broadband P wave analysis of the large deep Fiji Island and Bolivia earthquakes of 1994. *Geophysical research letters*, 22(16), 2249-2252.
- Gomer, B. M., & Okal, E. A. (2003). Multiple-ScS probing of the Ontong-Java plateau. *Physics of the Earth and Planetary Interiors*, 138(3), 317-331.
- Jordan, T. H., & Sipkin, S. A. (1977). Estimation of the attenuation operator for multiple ScS waves. *Geophysical Research Letters*, 4(4), 167-170.
- Kanamori, H., and Rivera, L. (2015). Near-vertical multiple ScS phases and vertically averaged mantle properties, in Foulger, G. R., Lustrino, M., and King, S. D., eds., *The Interdisciplinary Earth: A Volume in Honor of Don L. Anderson: Geological Society of America Special Paper 514 and American Geophysical Union Special Publication 71*, p. 9–31.
- Knopoff, L. (1964). A matrix method for elastic wave problems. *Bulletin of the Seismological Society of America*, 54(1), 431-438.
- Kovach, R. L., and Anderson, D. L. (1964). Attenuation of shear waves in the upper and lower mantle. *Bulletin of the Seismological Society of America*, 54(6A), 1855-1864.
- Lawrence, J. F., & Wyssession, M. E. (2006). QLM9: A new radial quality factor ( $Q_{\mu}$ ) model for the lower mantle. *Earth and Planetary Science Letters*, 241(3), 962-971.
- Lay, T., & Wallace, T. C. (1995). *Modern global seismology* (Vol. 58). Academic press.
- Mitchell, B. J., Baqer, S., Akinci, A., & Cong, L. (1998). Lg Coda Q in Australia and its Relation to Crustal Structure and Evolution. *Pure and Applied Geophysics*, 153(2-4), 639-653.
- Mitchell, B. J., Cong, L., & Ekström, G. (2008). A continent-wide map of 1-Hz Lg coda Q variation across Eurasia and its relation to lithospheric evolution. *Journal of Geophysical Research: Solid Earth (1978–2012)*, 113(B4).
- Nakanishi, I. (1979). Attenuation of multiple ScS waves beneath the Japanese arc. *Physics of the Earth and Planetary Interiors*, 19(4), 337-347.
- Nissen-Meyer, T., van Driel, M., Stähler, S. C., Hosseini, K., Hempel, S., Auer, L., ... & Fournier, A. (2014). AxiSEM: broadband 3-D seismic wavefields in axisymmetric media. *Solid Earth*, 5(1), 425-445.
- Ritsema, J., & van Heijst, H. J. (2002). Constraints on the correlation of P-and S-wave velocity heterogeneity in the mantle from P, PP, PPP and PKPab traveltimes. *Geophysical Journal International*, 149(2), 482-489.
- Ritsema, J., van Heijst, H. J., & Woodhouse, J. H. (1999). Complex shear wave velocity structure imaged beneath Africa and Iceland. *Science*, 286(5446), 1925-1928.
- Romanowicz, B., & Mitchell, B. (2007). Deep Earth structure: Q of the Earth from crust to core. *Treatise on geophysics*, 1, 731-774.

- Shito, A., & Shibutan, T. (2003). Anelastic structure of the upper mantle beneath the northern Philippine Sea. *Physics of the Earth and Planetary Interiors*, 140(4), 319-329.
- Suetsugu, D. (2001). A low QScS anomaly near the South Pacific Superswell. *Geophysical research letters*, 28(2), 391-394.
- Vallée, M., Charléty, J., Ferreira, A. M., Delouis, B., & Vergoz, J. (2011). SCARDEC: a new technique for the rapid determination of seismic moment magnitude, focal mechanism and source time functions for large earthquakes using body-wave deconvolution. *Geophysical Journal International*, 184(1), 338-358.
- Widmer, R., Masters, G., & Gilbert, F. (1991). Spherically symmetric attenuation within the Earth from normal mode data. *Geophysical journal international*, 104(3), 541-553.
- Xie, J., & Mitchell, B. J. (1990). A back-projection method for imaging large-scale lateral variations of Lg coda Q with application to continental Africa. *Geophysical Journal International*, 100(2), 161-181.